# Capture, Store, and Discharge. Shuttling Photogenerated Electrons across $TiO_2$–Silver Interface

**Azusa Takai[†] and Prashant V. Kamat***

Radiation Laboratory, Departments of Chemistry and Biochemistry and Chemical & Biomolecular Engineering, University of Notre Dame, Notre Dame, Indiana 46556, United States. [†]Present address: Department of Applied Chemistry, Faculty of Science and Engineering, Waseda University, 3-4-1 Ohkubo, Shinjuku-ku, Tokyo 169-8555, Japan.

**ABSTRACT** UV irradiation of $TiO_2$ nanoparticles in the presence of $Ag^+$ ions results in the quantitative reduction and deposition of silver on its surface. Continued UV irradiation following the deposition of Ag on the $TiO_2$ surface causes a blue shift in the surface plasmon peak from 430 to 415 nm as these particles become charged with excess electrons. Under UV irradiation, both the charging and discharging of electrons occur at different rates, thus allowing the system to attain a steady state. Upon stopping the UV irradiation, a fraction of these electrons remain stored. The electron storage is dependent on the amount of Ag deposited on $TiO_2$ nanoparticles with maximum capacity seen at 8.6 $\mu$M of Ag in a suspension containing 5.8 mM of $TiO_2$. Such electron charging and discharging processes in semiconductor–metal composites need to be taken into account while evaluating the plasmon resonance induced effects in photocatalysis and photoelectrochemistry.

**KEYWORDS:** semiconductor–metal composite · photocatalysts · $TiO_2$ · silver nanoparticles · plasmon resonance · solar energy conversion · electron storage

Semiconductor–metal nanocomposites are effective in facilitating photocatalytic processes.[1–9] The coupling of semiconductor and metal nanoparticles provides a unique pathway for the discharge of electrons at the electrolyte interface.[10–14] One such application of this process is in the photocatalytic production of hydrogen.[15,16] Many recent efforts of photocatalytic splitting of water require inclusion of a metal cocatalyst such as Pt.[17,18] The noble metals such as Au and Ag possess electron storage properties which in turn facilitates improved charge separation in semiconductor–metal composite systems.[19,20] Recent studies have also focused on surface plasmon excitation of metal nanoparticles and improvement in solar cell and photocatalytic performance of semiconductor–metal nanocomposites.[21–27] Although evidence is presented in these studies for observing electron injection from metal nanoparticles into semiconductor and/or plasmon resonance induced field effects, often these reported enhancements are small compared to the bulk semiconductor excitation effects.

Spectroscopic studies indicate that the electron transfer from a semiconductor to a metal nanoparticle is an ultrafast process.[28,29] For example, the electron transfer from CdSe into Pt occurs with a rate constant of $1.22 \times 10^9\ s^{-1}$.[28] While metals such as Pt and Pd provide an ohmic contact, metals such as Ag and Au exhibit capacitive properties. These coinage metals when they are small (2–5 nm in diameter) are capable of storing electrons.[30,31] Such electron storage causes a shift in the Fermi level. For example, earlier studies have shown that the shift in Fermi level could be as high as 0.1 V per stored electron.[32–35] The electron storage property can be beneficially used to improve the photoelectrochemical performance of nanostructured semiconductor films. In previous studies, we have shown that Au nanoparticles deposited on $TiO_2$ can directly participate in Fermi level equilibration under UV irradiation, thereby shifting the Fermi level of the composite to more negative potentials.[36–41] The stored electrons can be readily estimated by titrating with a known redox couple such as thionine or $C_{60}$. Smaller size particles were found to induce maximum shift in the Fermi level of the semiconductor–metal composite.

Another convenient way to probe the electron storage in metal nanoparticles is by monitoring its plasmon frequency. The addition of electrons to silver and gold nanoparticles or nanorods causes a blue shift in the absorption spectrum due to the increasing surface plasmon frequency of the electron gas.[41,42] The correlation between the number of stored electrons and the shift in plasmon frequency was compared in these studies. We have now utilized this property to establish the mechanism with which electron charge and discharge cycles operate in a semiconductor-assisted

* Address correspondence to pkamat@nd.edu.

Received for review June 21, 2011 and accepted August 5, 2011.

**Published online August 05, 2011**
**10.1021/nn202294b**

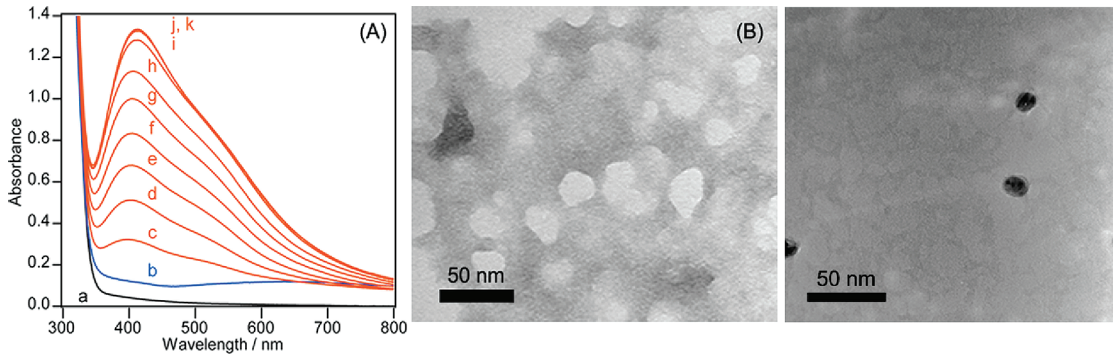


**Figure 1. (A) Absorption spectra of (a) deaerated and (b) UV-irradiated $TiO_2$ colloidal solution (5.8 mM, 3 mL) in ethanol (excitation Intensity ($\lambda$ > 300 nm) = 400 mW/cm$^2$), (c−k) incremental (0.1 mL) addition of 1.0 mM $AgNO_3$ to previously irradiated $TiO_2$ colloidal solution. (B) TEM image of $TiO_2$ (C) TEM image of $TiO_2$/Ag showing the deposition of Ag at few isolated $TiO_2$ particles.**

photocatalytic system. By monitoring the plasmon peak of the Ag, we have succeeded in elucidating the electron equilibration between $TiO_2$ and Ag nanoparticles.

## RESULTS AND DISCUSSION

**Reduction of $Ag^+$ Ions at the $TiO_2$ Interface.** The reduction of metal ions on the UV-irradiated $TiO_2$ surface has been the topic of extensive investigation since its first report by Bard and co-workers.[43] Whereas such metal deposition is beneficial in boosting the photocatalytic reduction processes by capturing the electrons from excited semiconductor nanoparticles, the presence of excess electrons also shifts the apparent Fermi level to more negative potentials.[2,3,39] In addition, the semiconductor/metal interface is dynamic as reduction of metal ions and oxidation of metal continues to proceed during UV irradiation of $TiO_2$.[44] In order to obtain a quantitative measure of the electron transfer to $Ag^+$ ions, we first irradiated the $TiO_2$ sample to trap electrons and then titrated trapped (or stored) electrons with externally added $Ag^+$ solution (previously deaerated) under $N_2$ atmosphere.

When the $TiO_2$ nanoparticle suspension in ethanol is subjected to UV irradiation, it turns blue as photogenerated electrons are trapped within $TiO_2$ at $Ti^{4+}$ sites. The holes are irreversibly scavenged by ethanol (reactions 1−3)

$$TiO_2 + h\nu \rightarrow TiO_2(e + h) \quad (1)$$

$$TiO_2(h) + C_2H_5OH \rightarrow TiO_2 + {}^{\bullet}C_2H_4OH \quad (2)$$

$$TiO_2(e) \rightarrow TiO_2(e_t) \quad (3)$$

In addition to photogenerated electrons, the alkoxy radicals ($^{\bullet}C_2H_4OH$) could also serve as reducing agent. Because of its low reduction potential, these alkoxy radicals cannot reduce $Ag^+$ in solution directly. However, they can indirectly contribute to the growth of Ag nanoparticles by transferring electrons to the Ag seed generated on the $TiO_2$ surface. Use of such mild reductants for controlled growth of metal nanoparticles has been demonstrated earlier.[45]

Absorption spectra, a and b, in Figure 1A show the absorbance of $TiO_2$ nanoparticles in ethanol before and after the UV irradiation. The broad absorbance in the 500−800 nm region correspond to trapped electrons. The trapping of the electrons in $TiO_2$ nanoparticles is quantitative, and the stored electrons can be titrated with electron acceptors such as $C_{60}$,[39] carbon nanotubes,[46] or graphene oxide.[47,48] In the present study, we employed $Ag^+$ ions to titrate stored electrons from $TiO_2$ nanoparticles. Incremental addition of $Ag^+$ ions resulted in the appearance of a new band at 410 nm (spectra c−k in Figure 1A). The absorption band which corresponds to Ag nanoparticles increases with increasing $Ag^+$ addition. As shown earlier, the initial seeds of silver nanoparticles grow with increasing addition of $Ag^+$ ions.[48] Once all of the electrons are scavenged by the $Ag^+$ ions, we see saturation in the plasmon absorption band (Figure 1A, spectra j and k). The amount of stored electrons as estimated from the silver ion titration was found to be 190 $\mu$M. The quantitative reduction of $Ag^+$ ions confirms the ability of trapped electrons to reduce $Ag^+$ ions and thus produce $TiO_2$/Ag composites.

**Charge and Discharge of Electrons during Steady State UV Irradiation.** In a previous study with Ag@$TiO_2$ core−shell particles, we have shown that the plasmon absorption band shifts from 480 to 420 nm as the electrons are stored in the Ag core.[41] Similar dependence of plasmon absorption band on the electron density was also established by treating metal nanoparticles with reducing agents.[42] In order to probe the electron storage effects, we carried out UV irradiation of $TiO_2$ in the presence of a known amount of $Ag^+$ in the suspension (86 $\mu$M). As expected, the $Ag^+$ ions are first reduced to Ag nanoparticles at the $TiO_2$ surface during the initial period of UV irradiation. The increase in plasmon band (435 nm) during first 8 min of irradiation confirms the formation of silver nanoparticles

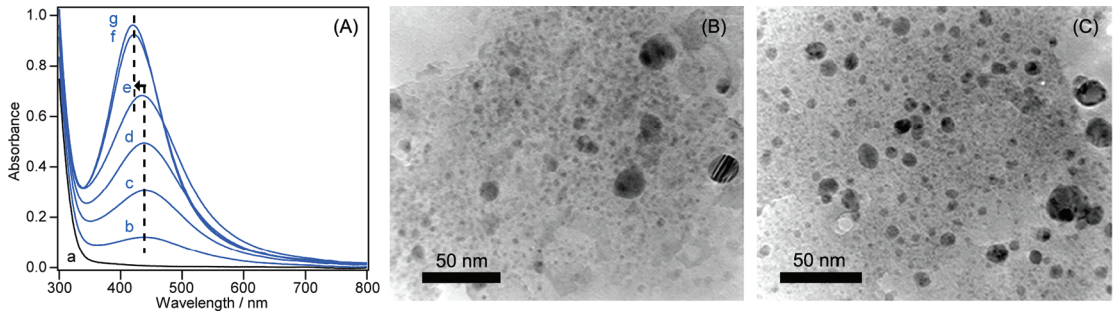


**Figure 2. (A) Absorption spectra of deaerated $TiO_2$ colloidal suspension (0.86 mM) and 86 $\mu$M of $AgNO_3$ in ethanol: (a) before irradiation and (b–g) during UV irradiation (spectra recorded at intervals of 2 min during irradiation, excitation Intensity ($\lambda$ > 300 nm) = 400 mW/cm$^2$). (B,C) TEM images of $TiO_2$–Ag samples at two different irradiation times (samples d and f from panel A).**

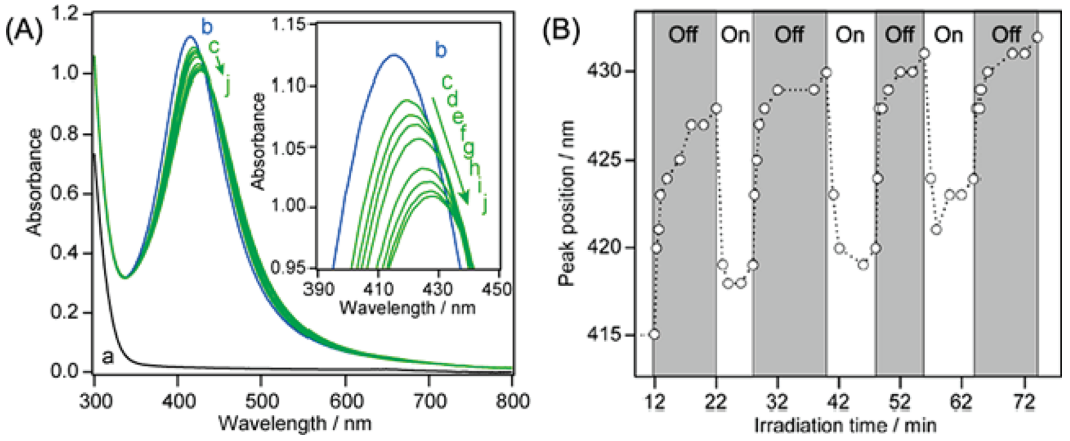


**Figure 3. (A) Absorption spectra of deaerated suspension of $TiO_2$ colloid (0.86 mM) and 86 $AgNO_3$ $\mu$M recorded (a) before and (b) after UV irradiation for 12 min. The spectra c–j were recorded after stopping the irradiation at intervals of 20 s, 40 s, 60 s, 2 min, 4 min, 6 min, 8 min, and 10 min, respectively. (B) Shift in the plasmon absorption peak during on–off cycles of irradiation. All experiments were conducted under nitrogen purge conditions.**

(Figure 2A, spectra a–e). No change in the plasmon peak position was observed during this initial period of illumination. As we continue the UV irradiation, the plasmon band increases further accompanied by a shift in the absorption peak position from 430 to 415 nm (Figure 2A, spectra f and g). This shift of ~15 nm in the plasmon absorption peak is representative of excess electrons stored within the Ag nanoparticle.

When the illumination was stopped, the plasmon peak slowly reverts back to 430 nm, indicating possible discharge of excess electrons at the electrolyte interface. The absorption spectra in Figure 3A show changes in the absorption peak upon stopping the UV illumination. We attribute this behavior to the existence of two separate equilibrium scenarios under illuminated and dark conditions, respectively (Scheme 1). If, indeed, these two dark and light equilibria are responsible for the shift in the plasmon peak, it should be possible to monitor them by subjecting the $TiO_2$/Ag system to on–off cycles of UV illumination.

Figure 3B shows the response of plasmon peak position during on–off cycles of UV irradiation of the

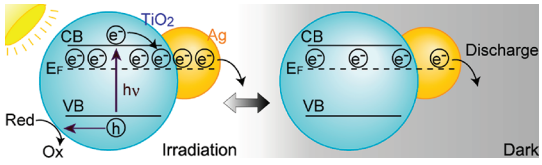


**Scheme 1. Charge equilibration scenarios between $TiO_2$ and Ag nanoparticles during continuous UV irradiation and in the dark.**

$TiO_2$/Ag system after completing the process of UV reduction of $Ag^+$ ions. The $N_2$ gas was continuously purged to maintain an inert atmosphere in the $TiO_2$/Ag suspension. It is interesting to note that the shift in the plasmon peak observed during UV irradiation of the $TiO_2$/Ag composite is reversible. Repeated on–off cycles exhibit a gradual shift of the plasmon band toward longer wavelengths. However, the peak position difference between the dark and illuminated conditions remains almost constant. Since the magnitude of the shift remains the same, we consider that the storage capacity of the $TiO_2$/Ag system is unaffected. At this time, we do not have concrete evidence for the red shift in the plasmon absorbance peak observed with continued irradiation cycles.

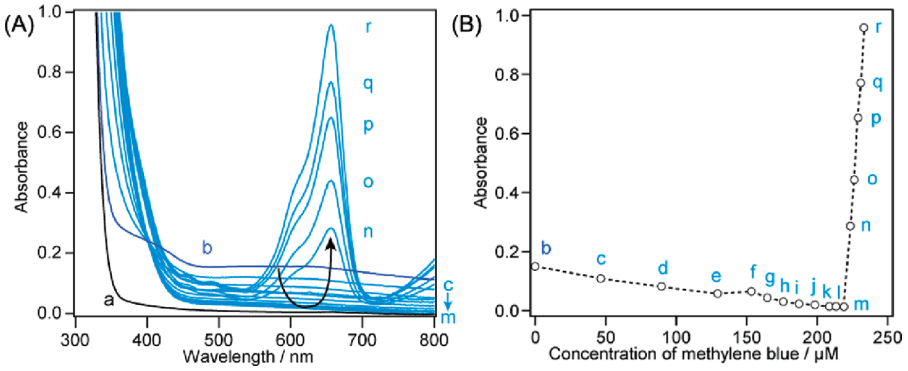


**Figure 4. (A) Absorption spectra of $TiO_2$ colloidal solution (5.8 mM) and $AgNO_3$ (8.6 $\mu$M) (a) before and (b) after irradiated solution saturated with $N_2$. The blue colored spectra (c−r) were recorded following incremental addition of MB to the suspension corresponding to "b" under $N_2$ atmosphere. (B) Titrations of stored electrons as measured from the changes in absorbance at 655 nm plotted are *versus* MB concentration.**

The stronger interaction of the $TiO_2$ and Ag deposit with continued UV irradiation and/or morphological changes can contribute to such a shift in the plasmon absorption band.

It is evident from these experiments that a steady state concentration of electrons is maintained within the Ag counterpart. We account for two competing processes (reactions 4 and 5) of charging and discharging processes that determine the net electrons stored during steady state UV irradiation.

$$TiO_2/Ag + h\nu \rightarrow TiO_2/Ag(ne) \quad (4)$$

$$TiO_2/Ag(ne) \rightarrow TiO_2/Ag(n - m)e + me \quad (5)$$

As long as the UV irradiation is continued, the forward reaction 4 continues to compensate for the electrons that are being discharged *via* reaction 5. As shown earlier, these excess electrons get discharged to reduce $H^+$ ions.[20,28] Once the UV irradiation is stopped, the system attains a dark equilibrium condition by discharging a fraction of the stored electrons. The remaining electrons stored within the Ag nanoparticles help maintain charge equilibration with $TiO_2$ nanoparticles in the dark. The apparent Fermi level, which is dependent on the electron concentration, ultimately dictates the transfer of electrons to the redox species at the interface. The reversible response of the absorbance peak position (Figure 3B) to UV irradiation thus shows that the charging and discharging of electrons through the metal deposits is a dynamic process. Such charging and discharging events have direct implications in the overall photocatalytic activity of semiconductor−metal nanocomposites.

**Estimation of the Electrons Stored after Stopping UV Illumination.** As expressed in reaction 5, a fraction of the electrons transferred during UV irradiation remains stored in the $TiO_2$/Ag composite even after stopping the irradiation. These electrons can be discharged by employing a redox potential that is more positive than the $H^+$ ion reduction potential. Thiazine dyes such as methylene blue (MB) with its reduction potential of 0.01 V *vs* NHE are found to be good electron acceptors.[46] The merit of such an electron titration method has been successfully demonstrated in earlier studies.[36,46,49] Methylene blue with its strong absorption at 655 nm ($\varepsilon$ = 10 000 $M^{-1}$ $cm^{-1}$) undergoes one electron reduction to form $MB^{-\bullet}$, which quickly disproportionates to yield a leuco dye, $MB^{2-}$ (reactions 6 and 7).

$$TiO_2/Ag(e^-) + MB \rightarrow TiO_2/Ag + MB^{-\bullet} \quad (6)$$

$$2MB^{-\bullet} \rightarrow MB^{2-} + MB \quad (7)$$

To the previously UV-irradiated $TiO_2$/Ag suspension was added a deaerated MB solution in fixed increments under $N_2$ atmosphere. Since the reduced methylene blue (leuco form) is colorless, we do not see any absorption of the dye at 655 nm (Figure 4A). With continued addition of methylene blue, the electrons are depleted from the $TiO_2$/Ag system. Once all of the stored electrons are extracted, further addition of MB causes a sudden increase in the 655 nm absorption. Figure 4B shows the changes in the absorbance at 655 nm with respect to the amount of electrons scavenged by MB. The breakpoint in the absorbance in Figure 4B is seen at 220 $\mu$M MB. Since the disappearance of each MB molecule corresponds to 2 electrons, this breakpoint corresponds to 440 $\mu$M electrons stored in the $TiO_2$/Ag system.

**Dependence of Electron Storage on the Amount of Silver Deposition.** As shown in the previous studies, the size of the metal nanoparticle affects the electron storage capacity and thus the overall shift in apparent Fermi level.[39] The double layer charging that screens the stored electrons within the metal nanoparticles is effective when the particles are relatively small (<10 nm diameter).[32] As discussed in the previous section (Figure 2), the silver particles grow on the $TiO_2$ surface during UV irradiation. Once a seed of Ag

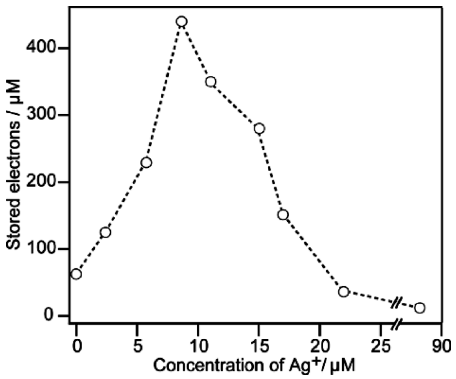


**Figure 5. Amount of stored electrons in $TiO_2$ nanoparticles (5.8 mM) containing different amounts of reduced $Ag^+$. The *x*-axis represents the initial $Ag^+$ added to the $TiO_2$ solution before UV irradiation.**

is formed on the $TiO_2$ surface, this seed catalyzes the reduction of $Ag^+$ ions. The size of the particle is thus proportional to [$Ag^+$]. Because of the difficulty in determining the exact size of these particles, we directly compared electron storage on the concentration of $Ag^+$. Extended period of UV irradiation ensured complete reduction of silver nanoparticles.

The $TiO_2$/Ag composites with different $TiO_2$:Ag composition ratios were prepared by varying the $Ag^+$ precursor concentration (0−86 $\mu$M) with constant $TiO_2$ concentration (5.8 mM). Extended periods of UV illumination ensured complete reduction of $Ag^+$. After dark equilibration, the $TiO_2$/Ag composites were subjected to UV irradiation for a fixed time duration under $N_2$ atmosphere. After the UV irradiation was stopped, the suspension was allowed to re-equilibrate in the dark and the stored electrons were titrated with MB. The amount of stored electrons *versus* $Ag^+$ concentration is presented in Figure 5. We see an increased amount of electron storage as we increased deposition of Ag on the $TiO_2$ surface. The maximum electron storage of 440 $\mu$M is seen when $Ag^+$ concentration employed for the deposition of Ag was 8.6 $\mu$M. At higher Ag concentrations, we see a decrease in the electron storage capacity. This decreasing trend seen at higher silver concentration (as represented by reduced [$Ag^+$]) is attributed to two factors. (i) The larger size metal nanoparticles are less effective in storing electrons and shifting the Fermi level to more negative potentials. (ii) Since outer Ag layer absorbs strongly in the UV, the light filtration effect reduces the probability of direct excitation and creating charge separation.

We also extended this strategy to probe the electron storage effect of other metals. Deposition of Ag, Au, and Pt was carried out by adding the same amount of metal ion precursor to $TiO_2$ suspensions and subjecting them to UV irradiation. Change in the UV absorption was monitored to follow the metal deposition. (Because of the absence of surface plasmon band, we followed Pt deposition by change in the absorbance at 350 nm.) After the deposition of respective metals, the samples were exposed to air so that the stored electrons are scavenged by oxygen. The suspensions containing $TiO_2$−metal composites were deaerated and subjected to UV irradiation for a fixed time. The stored electrons in each of these composites were estimated using the methylene blue titration. The values of stored electrons in the three composite systems are presented in Table 1. The relative comparison of the values suggests that $TiO_2$/Ag is most effective in storing electrons. Noble metals such as Ag and Au are known to possess capacitive behavior. However, precious metals such as Pt and Pd are ohmic in nature, thereby exhibiting less storage capacity. Such an ohmic behavior renders quick discharge of electrons at the electrolyte interface. The electron discharge capacity of Pt nanoparticles and its role in photocatalytic reduction is discussed in detail in a recent study.[28]

**TABLE 1. Electron Storage in $TiO_2$ Modified with Different Metals[a]**

| metal | stored electrons/$\mu$M |
|---|---|
| none | 63 |
| Ag | 440 |
| Au | 280 |
| Pt | 190 |

[a] $TiO_2$ suspension (5.8 mM) containing 8.6 $\mu$M metal precursor was irradiated to carry out deposition of the corresponding metal.

**Fermi Level Equilibration.** As shown in earlier studies, semiconductor and metal nanoparticles undergo electron equilibration when subjected to band gap irradiation.[31,36,39] Since the Fermi level of metals such as Ag ($E_F$ = 0.45 V *vs* SCE) is more positive than the conduction band of $TiO_2$, the photogenerated electrons are transferred to Ag nanoparticles. If the electrons remain stored within the Ag nanoparticle, its Fermi level shifts to more negative potentials. For example, we have shown that quantized charging of metal nanoparticles results in the shift of apparent Fermi level of the $TiO_2$/Au composite to more negative potentials (up to ~100 mV). In the present experiments, we estimated the apparent Fermi level of the $TiO_2$/Ag composite by equilibrating a previously irradiated $TiO_2$/Ag suspension with a $MB^{2-}$/MB redox couple. After allowing the system to equilibrate, we determined the reduced and unreduced form of the MB. By employing the Nernst equation, we could then calculate the apparent Fermi level of the $TiO_2$/Ag composite system.

$$E_F = E^0 + 0.059/2 \log([MB]/[MB^{2-}])$$

where $E^0$ is the two electron reduction potential of the MB/$MB^{2-}$ couple ($E^0$ = 0.01 V *vs* NHE). In the present experiments (for example, at the end of the titration experiment in Figure 4), the reduced and oxidized forms of the MB correspond to 220 and 10 $\mu$M, respectively. The apparent Fermi level of the $TiO_2$/Ag system thus

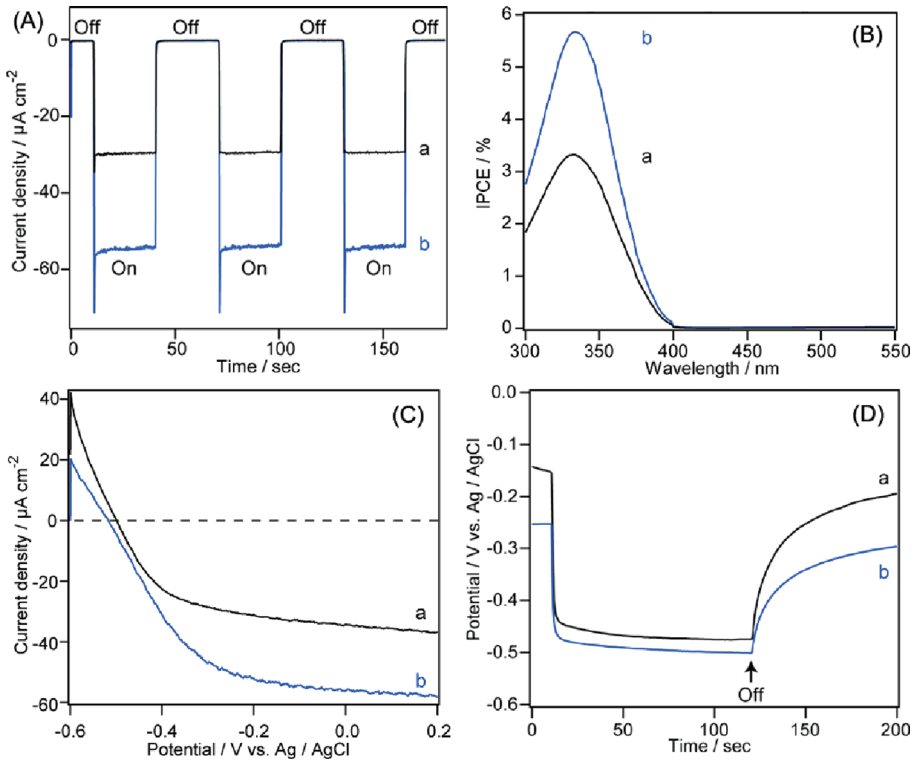


**Figure 6. (A) Photocurrent response, (B) IPCE, (C) current−voltage curves, and (D) $V_{oc}$ time profiles of (a) $TiO_2$ and (b) $TiO_2$/Ag films with $TiO_2$:Ag composition ratio corresponding to the maximum electron storage in Figure 5.**

corresponds to −0.03 V *vs* NHE. Although the magnitude of this shift is small (~40 mV), the stored electrons in Ag allows for a more reductive energy level for the composite system to be maintained, and this in turn renders improved photocatalytic property.

**Implication of Electron Storage on the Photoelectrochemical Performance of $TiO_2$/Ag Films.** One of the major limiting factor in attaining higher photovoltage in nanostructured semiconductor-based photoelectrochemical cells is the losses due to charge recombination process at the photoanode. It is necessary to increase electron accumulation within the semiconductor film if one is interested in attaining more negative Fermi level (and hence greater photovoltage). The electron storage within the Ag nanoparticles should assist in attaining a more negative Fermi level at the $TiO_2$/Ag film as compared to plain $TiO_2$ electrode. If indeed the stored electrons in the $TiO_2$/Ag composite assist in maintaining a more negative Fermi level than the pristine $TiO_2$, it should reflect in the improved photoelectrochemical performance.

Many of the recent studies have reported small enhancements in photocurrents upon excitation of the surface plasmon band in semiconductor−metal nanocomposites.[22−27,50] The photoresponse in the visible plasmon absorption band of the corresponding metal is presented as evidence to show their direct participation *via* the process of electron injection from metal nanoparticles into semiconductor and/or field effect induced by plasmon resonance. Even if such plasmon-enhanced photoconversion plays a role, its contribution to overall photoelectrochemical performance has remained quite low.

To further elucidate the electron storage effect, we compared the photoelectrochemical behavior of $TiO_2$ and $TiO_2$/Ag films. We prepared $TiO_2$/Ag film on an ITO substrate by depositing first a mesoscopic $TiO_2$ film from solvent evaporation of $TiO_2$ colloidal solution and then exposing the annealed film to $Ag^+$ solution and UV light. Photoreduction of $Ag^+$ ions at the $TiO_2$ surface produces $TiO_2$/Ag films. The ratio of $TiO_2$:Ag was maintained at the same level as that of the sample shown in Figure 4. The photocurrent response of $TiO_2$ and $TiO_2$/Ag recorded at 0 V *vs* Ag/AgCl is shown in Figure 6A. The photocurrent remained stable during irradiation, and the current density did not decrease after three cycles. The photocurrent of $TiO_2$/Ag was about 2 times higher than that of pristine $TiO_2$. The incident photon to current conversion efficiency (IPCE) was measured from short circuit photocurrent ($I_{sc}$) measurements at different wavelengths ($\lambda$) and incident light power ($I_{inc}$) using the following equation.

$$\mathrm{IPCE}(\%) = (1240 \times I_{sc}(\mathrm{Acm}^{-2}))/(\lambda(\mathrm{nm}) \times I_{inc}(\mathrm{Wcm}^{-2})) \times 100$$

The onset wavelength for the photocurrent generation and the wavelength corresponding to maximum IPCE ($\lambda$ = 335 nm) of $TiO_2$/Ag are similar to those seen for pristine $TiO_2$ electrodes (Figure 6B). The photocurrent

response corresponding to the wavelength of surface plasmon resonance of Ag (viz., in the range of 415–430 nm) was negligible. These results further confirm our assertion that direct excitation of Ag nanoparticles plays negligible effect in the photocurrent generation at the $TiO_2$/Ag electrode. The current–voltage curves of $TiO_2$ and $TiO_2$/Ag films shown in Figure 6C indicate that the zero-current potential of the $TiO_2$/Ag electrode shifts to negative potentials as compared to $TiO_2$. As discussed in the previous section, electron storage in the Ag shell drives the Fermi level to more negative potential and thus increases the open circuit voltage. In addition to the beneficial aspect of Fermi level equilibration, the presence of silver also improves the charge separation. The open circuit voltage recorded upon stopping the illumination (Figure 6D) shows a slower decay when Ag was present at the electrolyte interface. These photoelectrochemical measurements further ascertain the importance of electron storage effect of metal deposits in improving the photoelectrochemical properties of mesoscopic semiconductor films.

## CONCLUSIONS

Semiconductor nanoparticles coupled with metals are known to exhibit photocatalytic properties. The recent efforts to explore plasmon resonance effect to influence charge separation efficiencies in photocatalytic systems often undermine the electron acceptor properties of metal nanoparticles. The results presented here demonstrate that photocatalytically deposited Ag on $TiO_2$ nanoparticles improves the photoelectrochemical performance of the $TiO_2$/Ag composite by capturing the photogenerated electrons and maintaining a more negative Fermi level. The shift in the plasmon resonance of Ag shows that the charge equilibration between $TiO_2$ and Ag is dependent on the irradiation conditions. The charging and discharging can be reversibly modulated through on–off cycles of UV irradiation. These electron storage effects should be taken into consideration while evaluating the photocatalytic and photoelectrochemical properties of semiconductor–metal composites.

## EXPERIMENTAL SECTION

**Materials and Methods.** Titanium isopropoxide and ethanol (200 proof) were purchased from Acros Organics and Decon Laboratories Inc., respectively. Silver nitrate and glacial acetic acid were purchased from Fisher Scientific. Methylene blue, dihydrogen hexachloroplatinate(IV) hexahydrate, hydrogen tetrachloroaurate(III) trihydrate, and ruthenium(III) chloride were purchased from Aldrich. Indium tin oxide coated glass plates (ITO, 1.3 mm thick, 20 Ω/□) were obtained from Pilkington Glass Co., Toledo, OH.

$TiO_2$ colloidal nanoparticles were prepared by adding dropwise 0.1 mL of titanium isopropoxide into 39.9 mL of ethanol under stirring. The colloidal solution was stirred continuously prior to use. UV irradiation for selective photoexcitation of $TiO_2$ and reduction of $Ag^+$ was performed using an Eimac xenon arc lamp (300 W) with a $CuSO_4/H_2O$ filter or a monochromator ($\lambda$ = 300 nm). Unless otherwise indicated, all of the solutions were purged with $N_2$ gas continuously during irradiation and during storage.

**Measurements.** UV–vis absorption spectra were measured with Varian Cary 50-Bio UV–visible spectrophotometer. Transmission electron microscopic (TEM) images were recorded using JEOL 2010 microscope. Photoelectrochemical measurements were carried out with $TiO_2$/Ag films prepared on ITO substrates. $TiO_2$ films, which were prepared by drop-casting of $TiO_2$ colloidal nanoparticles and annealed at 450 °C for 1 h, were irradiated in a deaerated $AgNO_3$ aqueous solution to deposit Ag nanoparticles.

Photoelectrochemical measurements were carried out in a three electrode cell consisting of a platinum gauze counter electrode and a KCl saturated Ag/AgCl reference electrode in 0.01 M of KOH aqueous solution using a Princeton Applied Research potentiostat PARSTAT 2263. Measurements were conducted using a 150 W xenon arc lamp adopted with an AM 1.5 filter as a white light source.

*Acknowledgment.* The research described herein was supported by the Division of Chemical Sciences, Geosciences and Biosciences, Office of Basic Energy Sciences of the U.S. Department of Energy through Grant DE-FC02-04ER15533. This is contribution number NDRL 4890 from the Notre Dame Radiation Laboratory. We thank Mr. Ian Lightcap for his assistance in recording TEM images. A.T. acknowledges the guidance of Prof. Kazuyuki Kuroda (Waseda University) and the financial support provided through a Grant-in-Aid for JSPS Fellow and Excellent Young Researchers Overseas Visit Program of JSPS.

## REFERENCES AND NOTES

1. Henglein, A. Small-Particle Research: Physicochemical Properties of Extremely Small Colloidal Metal and Semiconductor Particles. *Chem. Rev.* **1989**, *89*, 1861–1873.
2. Henglein, A. Physicochemical Properties of Small Metal Particles in Solution: "Microelectrode" Reactions, Chemisorption, Composite Metal Particles, and the Atom-to-Metal Transition. *J. Phys. Chem.* **1993**, *97*, 5457–5471.
3. Kamat, P. V. Photophysical, Photochemical and Photocatalytic Aspects of Metal Nanoparticles. *J. Phys. Chem. B* **2002**, *106*, 7729–7744.
4. Matsumura, M.; Saho, Y.; Tsubomura, H. Photocatalytic Hydrogen Production from Solutions of Sulfite Using Platinized Cadmium Sulfide Powder. *J. Phys. Chem.* **1983**, *87*, 3807–3808.
5. Nosaka, Y.; Yamaguchi, K.; Kuwabara, A.; Miyama, H.; Baba, R.; Fujishima, A. Colloidal CdS–Pt Photocatalyst Stabilized by Pendant Viologen Polymer for Photoinduced Electron Transfer and Hydrogen Evolution. *J. Photochem. Photobiol., A* **1992**, *64*, 375–382.
6. Jin, Z.; Li, Q.; Zheng, X.; Xi, C.; Wang, C.; Zhang, H.; Feng, L.; Wang, H.; Chen, Z.; Jiang, Z. Surface Properties of Pt–CdS and Mechanism of Photocatalytic Dehydrogenation of Aqueous Alcohol. *J. Photochem. Photobiol., A* **1993**, *71*, 85–96.
7. Kudo, A.; Miseki, Y. Heterogeneous Photocatalyst Materials for Water Splitting. *Chem. Soc. Rev.* **2009**, *38*, 253–278.
8. Shankar, K.; Basham, J. I.; Allam, N. K.; Varghese, O. K.; Mor, G. K.; Feng, X.; Paulose, M.; Seabold, J. A.; Choi, K.-S.; Grimes, C. A. Recent Advances in the Use of $TiO_2$ Nanotube and Nanowire Arrays for Oxidative Photoelectrochemistry. *J. Phys. Chem. C* **2009**, *113*, 6327–6359.
9. Ng, Y. H.; Iwase, A.; Kudo, A.; Amal, R. Reducing Graphene Oxide on a Visible-Light $BiVO_4$ Photocatalyst for an

Enhanced Photoelectrochemical Water Splitting. *J. Phys. Chem. Lett.* **2010**, *1*, 2607–2612.
10. Kiwi, J.; Graetzel, M. Protection, Size Factors, and Reaction Dynamics of Colloidal Redox Catalysts Mediating Light Induced Hydrogen Evolution from Water. *J. Am. Chem. Soc.* **1979**, *101*, 7214–7217.
11. Henglein, A.; Lindig, B.; Westerhausen, J. Photochemical Electron Storage on Colloidal Metals and Hydrogen Formation by Free Radicals. *J. Phys. Chem.* **1981**, *85*, 1627–1628.
12. Lee, P. C.; Matheson, M. S.; Meisel, D. Photogeneration of Hydrogen from Polymeric Viologen Systems. *Isr. J. Chem.* **1982**, *22*, 133–137.
13. Matheson, M. S.; Lee, P. C.; Meisel, D.; Pelizzetti, E. Kinetics of Hydrogen Production from Methyl Viologen Radicals on Colloidal Platinum. *J. Phys. Chem.* **1983**, *87*, 394–399.
14. Aspnes, D. E.; Heller, A. Photoelectrochemical Hydrogen Evolution and Water-Photolyzing Semiconductor Suspensions: Properties of Platinum Group Metal Catalyst–Semiconductor Contacts in Air and in Hydrogen. *J. Phys. Chem.* **1983**, *87*, 4919–4929.
15. Maeda, K.; Domen, K. Photocatalytic Water Splitting: Recent Progress and Future Challenges. *J. Phys. Chem. Lett.* **2010**, *1*, 2655–2661.
16. Joshi, U. A.; Palasyuk, A.; Arney, D.; Maggard, P. A. Semiconducting Oxides To Facilitate the Conversion of Solar Energy to Chemical Fuels. *J. Phys. Chem. Lett.* **2010**, *1*, 2719–2726.
17. Amirav, L.; Alivisatos, A. P. Photocatalytic Hydrogen Production with Tunable Nanorod Heterostructures. *J. Phys. Chem. Lett.* **2010**, *1*, 1051–1054.
18. Wang, C.; Thompson, R. L.; Baltrus, J.; Matranga, C. Visible Light Photoreduction of $CO_2$ Using CdSe/Pt/$TiO_2$ Heterostructured Catalysts. *J. Phys. Chem. Lett.* **2010**, *1*, 48–53.
19. Shanghavi, B.; Kamat, P. V. Interparticle Electron Transfer in Metal/Semiconductor Composites. Picosecond Dynamics of CdS Capped Gold Nanoclusters. *J. Phys. Chem. B* **1997**, *101*, 7675–7679.
20. Merga, G.; Cass, L. C.; Chipman, D. M.; Meisel, D. Probing Silver Nanoparticles during Catalytic $H_2$ Evolution. *J. Am. Chem. Soc.* **2008**, *130*, 7067–7076.
21. Tian, Y.; Tatsuma, T. Mechanisms and Applications of Plasmon-Induced Charge Separation at $TiO_2$ Films Loaded with Gold Nanoparticles. *J. Am. Chem. Soc.* **2005**, *127*, 7632–7637.
22. Devadas, M. S.; Kwak, K.; Park, J.-W.; Choi, J.-H.; Jun, C.-H.; Sinn, E.; Ramakrishna, G.; Lee, D. Directional Electron Transfer in Chromophore-Labeled Quantum-Sized Au25 Clusters: Au25 as an Electron Donor. *J. Phys. Chem. Lett.* **2010**, *1*, 1497–1503.
23. Nishijima, Y.; Ueno, K.; Yokota, Y.; Murakoshi, K.; Misawa, H. Plasmon-Assisted Photocurrent Generation from Visible to Near-Infrared Wavelength Using a Au-Nanorods/$TiO_2$ Electrode. *J. Phys. Chem. Lett.* **2010**, *1*, 2031–2036.
24. Standridge, S. D.; Schatz, G. C.; Hupp, J. T. Distance Dependence of Plasmon-Enhanced Photocurrent in Dye-Sensitized Solar Cells. *J. Am. Chem. Soc.* **2009**, *131*, 8407–8409.
25. Standridge, S. D.; Schatz, G. C.; Hupp, J. T. Toward Plasmonic Solar Cells: Protection of Silver Nanoparticles *via* Atomic Layer Deposition of $TiO_2$. *Langmuir* **2009**, *25*, 2596–2600.
26. Brown, M. D.; Suteewong, T.; Kumar, R. S. S.; D'Innocenzo, V.; Petrozza, A.; Lee, M. M.; Wiesner, U.; Snaith, H. J. Plasmonic Dye-Sensitized Solar Cells Using Core@Shell Metal@Insulator Nanoparticles. *Nano Lett.* **2011**, *11*, 438–445.
27. Liu, Z.; Hou, W.; Pavaskar, P.; Aykol, M.; Cronin, S. B. Plasmon Resonant Enhancement of Photocatalytic Water Splitting under Visible Illumination. *Nano Lett.* **2011**, *11*, 1111–1116.
28. Harris, C.; Kamat, P. V. Photocatalytic Events of CdSe Quantum Dots in Confined Media. Electrodic Behavior of Coupled Platinum Nanoparticles. *ACS Nano* **2010**, *4*, 7321–7330.
29. Katoh, R.; Furube, A.; Yamanaka, K.-i.; Morikawa, T. Charge Separation and Trapping in N-Doped $TiO_2$ Photocatalysts: A Time-Resolved Microwave Conductivity Study. *J. Phys. Chem. Lett.* **2010**, *1*, 3261–3265.
30. Henglein, A.; Holzwarth, A.; Mulvaney, P. Fermi Level Equilibration between Colloidal Lead and Silver Particles in Aqueous Solution. *J. Phys. Chem.* **1992**, *96*, 8700–8702.
31. Wood, A.; Giersig, M.; Mulvaney, P. Fermi Level Equilibration in Quantum Dot–Metal Nanojunctions. *J. Phys. Chem. B* **2001**, *105*, 8810–8815.
32. Chen, S.; Ingram, R. S.; Hostetler, M. J.; Pietron, J. J.; Murray, R. W.; Schaaff, T. G.; Khoury, J. T.; Alvarez, M. M.; Whetten, R. L. Gold Nanoelectrodes of Varied Size: Transition to Molecule-like Charging. *Science* **1998**, *280*, 2098–2101.
33. Chen, S.; Murray, R. W.; Feldberg, S. W. Quantized Capacitance Charging of Monolayer-Protected Au Clusters. *J. Phys. Chem. B* **1998**, *102*, 9898–9907.
34. Chen, S.; Murray, R. W. Electrochemical Quantized Capacitance Charging of Surface Ensembles of Gold Nanoparticles. *J. Phys. Chem. B* **1999**, *103*, 9996–10000.
35. Templeton, A. C.; Wuelfing, W. P.; Murray, R. W. Monolayer Protected Cluster Molecules. *Acc. Chem. Res.* **2000**, *33*, 27–36.
36. Jakob, M.; Levanon, H.; Kamat, P. V. Charge Distribution between UV-Irradiated $TiO_2$ and Gold Nanoparticles. Determination of Shift in Fermi Level. *Nano Lett.* **2003**, *3*, 353–358.
37. Subramanian, V.; Wolf, E.; Kamat, P. V. Semiconductor–Metal Composite Nanostructures. To What Extent Do Metal Nanoparticles (Au, Pt, Ir) Improve the Photocatalytic Activity of $TiO_2$ Films? *J. Phys. Chem. B* **2001**, *105*, 11439–11446.
38. Subramanian, V.; Wolf, E. E.; Kamat, P. V. Green Emission To Probe Photoinduced Charging Events in ZnO–Au Nanoparticles. Charge Distribution and Fermi-Level Equilibration. *J. Phys. Chem. B* **2003**, *107*, 7479–7485.
39. Subramanian, V.; Wolf, E. E.; Kamat, P. V. Catalysis with $TiO_2$/Au Nanocomposites. Effect of Metal Particle Size on the Fermi Level Equilibration. *J. Am. Chem. Soc.* **2004**, *126*, 4943–4950.
40. Hirakawa, T.; Kamat, P. V. Electron Storage and Surface Plasmon Modulation in Ag@$TiO_2$ Clusters. *Langmuir* **2004**, *20*, 5645–5647.
41. Hirakawa, T.; Kamat, P. V. Charge Separation and Catalytic Activity of Ag@$TiO_2$ Core–Shell Composite Clusters under UV-Irradiation. *J. Am. Chem. Soc.* **2005**, *127*, 3928–3934.
42. Novo, C.; Mulvaney, P. Charge-Induced Rayleigh Instabilities in Small Gold Rods. *Nano Lett.* **2007**, *7*, 520–524.
43. Dunn, W. W.; Aikawa, Y.; Bard, A. J. Heterogeneous Photosynthetic Production of Amino Acids at Pt/$TiO_2$ Suspensions by Near Ultraviolet Light. *J. Am. Chem. Soc.* **1981**, *103*, 6893–6897.
44. Subramanian, V.; Wolf, E. E.; Kamat, P. V. Influence of Metal/Metal-Ion Concentration on the Photocatalytic Activity of $TiO_2$–Au Composite Nanoparticles. *Langmuir* **2003**, *19*, 469–474.
45. Henglein, A.; Meisel, D. Radiolytic Control of the Size of Colloidal Gold Nanoparticles. *Langmuir* **1998**, *14*, 7392–7396.
46. Kongkanand, A.; Kamat, P. V. Electron Storage in Single Wall Carbon Nanotubes. Fermi Level Equilibration in Semiconductor–SWCNT Suspensions. *ACS Nano* **2007**, *1*, 13–21.
47. Williams, G.; Seger, B.; Kamat, P. V. $TiO_2$-Graphene Nanocomposites. UV-Assisted Photocatalytic Reduction of Graphene Oxide. *ACS Nano* **2008**, *2*, 1487–1491.
48. Lightcap, I. V.; Kosel, T. H.; Kamat, P. V. Anchoring Semiconductor and Metal Nanoparticles on a Two-Dimensional Catalyst Mat. Storing and Shuttling Electrons with Reduced Graphene Oxide. *Nano Lett.* **2010**, *10*, 577–583.
49. Kongkanand, A.; Kamat, P. V. Interactions of Single Wall Carbon Nanotubes with Methyl Viologen Radicals. Quantitative Estimation of Stored Electrons. *J. Phys. Chem. C* **2007**, *111*, 9012–9015.
50. Kulkarni, A. P.; Noone, K. M.; Munechika, K.; Guyer, S. R.; Ginger, D. S. Plasmon-Enhanced Charge Carrier Generation in Organic Photovoltaic Films Using Silver Nanoprisms. *Nano Lett.* **2010**, *10*, 1501–1505.